Radiation Measurements 159 (2022) 106875

Contents lists available at ScienceDirect

Radiation Measurements

journal homepage: www.elsevier.com/locate/radmeas

Characterisation of a monolithic *ΔE-E* diamond telescope detector using low energy ion microbeams

C. Verona [a], G. Parisi [b,c,*], S. Cesaroni [a], A. Crnjac [d], M. Jakšić [d], M. Marinelli [a], S. Palomba [a], F. Romano [e], G. Schettino [b,c], G. Verona Rinati [a]

[a] *Dipartimento di Ingegneria Industriale, Università di Roma "Tor Vergata", Via del Politecnico 1, 00133, Roma, Italy*
[b] *Department of Physics, University of Surrey, Guildford, GU2 7XH, UK*
[c] *National Physical Laboratory - NPL, Hampton Road, Teddington, TW11 0LW, UK*
[d] *Laboratory for Ion Beam Interactions, Ruđer Bošković Institute, Bijenicka Cesta 54, 10000, Zagreb, Croatia*
[e] *Istituto Nazionale di Fisica Nucleare - INFN, sezione di Catania, Catania, Italy*

A B S T R A C T

Telescope detectors have long been studied for their capability of discriminating the type of radiation detected. Silicon is the most widely used material for solid-state detectors. However, in many nuclear physics experiments and medical applications, diamond offers significant advantages due to its outstanding features, such as a near tissue equivalence, high radiation hardness and reliable operation in harsh environments.

A monolithic ΔE–E diamond-based telescope was fabricated. The thicknesses of the two detection stages were 2.5 μm and 500 μm for the ΔE and E stage, respectively. The device was characterised by means of IBIC (Ion Beam Induced Charge) analysis at the Ruđer Bošković Institute ion microbeam. The detector, irradiated with different low energy ions ranging from helium to oxygen, showed good homogeneity of the response on a well-defined sensitive volume with a charge collection efficiency close to 100%.

The ΔE stage showed a very good linear response on a wide range of LET values in diamond (170–3140 keV/μm). Due to its relatively low thickness, it can be successfully used as a microdosimeter.

Time coincidence measurements have demonstrated the diamond telescope capability of discriminating and identifying the impinging ions. However, when the ratio between the energy deposited by the particle in the E stage and in the ΔE stage is small, the response of the E stage was observed to be affected by a cross-talk between the two stages of the device. A method to correct the E response for such effect was developed and successfully applied to the acquired data.

1. Introduction

ΔE–E telescope detectors are developed for charged particle identification and energy measurements in high-energy particle physics, nuclear physics experiments and space research as well as medical applications (Agosteo et al., 2014, 2008; Carboni et al., 2012; Ciampi et al., 2019; Guan et al., 2022; Gunzert-Marx et al., 2004; Jin et al., 2013; Ma et al., 2016; Matsufuji et al., 2003; Mitcuk and Mordovskoy, 2019; Gabriele Parisi et al., 2022; Wroe et al., 2009). A *ΔE-E* telescope is a multi-layer detection system consisting of a first detector (called *ΔE*), characterised by a thickness shorter than the range of the charged particle to be detected, and a second detector (called *E*), situated behind the first detector, with a thickness generally larger than the residual range of the particle. Therefore, the impinging particles pass through the first detector and stop in the second one. The partition of energy deposited in the two detectors is unique of the type of particle, due to the different stopping power of each particle type. The energies deposited in both detectors are measured in time coincidence and are usually depicted in a *ΔE-E* scatter plot. Each event produced by a certain charged particle type occupies a well-defined zone on this plot, which is used for particle identification. The thicknesses of the ΔE and *E* detectors are chosen according to the suitability in the detection of charged particles of different energy in mixed radiation fields.

Solid state telescope detectors for the identification of ions and fission fragments coming from nuclear reactions are reported in literature for several applications (Ahmadov et al., 2015; Gunzert-Marx et al., 2008; Kramer et al., 2016; Matsufuji et al., 2005; Mazzucconi et al., 2021; Mueller et al., 1988; Pasquali et al., 2014; Topkar et al., 2011; Tran et al., 2018) showing high energy resolutions as well as good particle identification capabilities. Such detectors are mainly based on silicon (Si) technology. This is because Si is simple to be manufactured, cheap and its properties are well known. However, new frontiers in physics such as those found in nuclear reactors, particle accelerators or in outer space, featured by extreme radiation fluxes and temperature

* Corresponding author. Department of Physics, University of Surrey, Guildford, GU2 7XH, UK.
E-mail address: g.parisi@surrey.ac.uk (G. Parisi).

https://doi.org/10.1016/j.radmeas.2022.106875
Received 3 August 2022; Received in revised form 13 October 2022; Accepted 31 October 2022
Available online 9 November 2022

conditions will exceed the limits of some conventional radiation diagnostics based on silicon. Thanks to their unique electronic and physical properties (Gabrysch et al., 2011; Isberg et al., 2002; Pomorski et al., 2007), synthetic single-crystal diamonds grown using the chemical vapor deposition (CVD) technique are good candidates for those future applications and they are currently investigated as an alternative to silicon.

The wide bandgap of diamond (5.5 eV) assures detectors to exhibit low leakage current and to be capable of operating at high temperatures. The small dielectric constant (5.6) leads to devices with small capacitance and low noise operation. On the other hand, the amount of energy to create an electron-hole pair in diamond (13 eV) compared with silicon (3.6 eV) results in a comparable decrease in sensitivity and energy resolution. The atom displacement energy (43 eV) allows long-term operations in harsh environments, presenting an excellent resistance to radiation almost one order of magnitude larger than silicon (de Boer et al., 2007). Moreover, the low atomic number of diamond ($Z = 6$) implies tissue equivalence for photons, that could be extended to protons and carbon ions thanks to the near-constant ratio of stopping power of diamond with water for such ions. This makes diamond-based detectors particularly attractive for medical radiation dosimetry and microdosimetry applications(Davis et al., 2017; Verona et al., 2018; Zahradnik et al., 2018).

The fabrication and preliminarily characterization of a first *ΔE-E* diamond telescope detector using 5.5 MeV α-particle was recently reported (Cesaroni et al., 2019). This kind of detector is fabricated with a thickness of *ΔE* stage of the order of few microns making it particularly useful for detecting low energy ions which are representative for therapeutic beams at the end of their path and for microdosimetry of therapeutic ion beams. Indeed, the *ΔE-E* diamond telescope detector can be used at the same time as a microdosimeter for a particle by particle characterization of ion beams and as a detector for products deriving from nuclear fragmentation of the primary ions. This is extremely useful when characterising mixed radiation fields found around and at the distal part of the Bragg Peak of a typical clinical ion beam.

In this paper, a *ΔE-E* diamond telescope was further characterised at the Ruđer Bošković Institute (RBI, Zagreb, Croatia) ion microprobe facility using the Ion Beam Induced Charge (IBIC) technique to investigate its charge collection efficiency, its spectroscopic properties, the homogeneity of its response as well as its potential as a particle discriminator. The characteristics of the detector were studied using different ion species and beam energies, associated with different values of Linear Energy Transfer (LET) in diamond. The experimental results were also analysed in terms of Monte Carlo simulations by means of Geant 4.

2. Materials and methods

2.1. Fabrication of ΔE-E diamond detector

The detector characterised in this experiment is a monolithic *ΔE-E* diamond telescope detector, which consists of two Schottky diodes both manufactured on a single diamond plate. The top *ΔE* detector and bottom *E* detector share a heavily boron doped diamond film.

The E detector is an electronic grade single-crystal CVD diamond provided by Element Six (https://e6cvd.com/). The size of the diamond plate is 2×2 mm^2 with a thickness of 500 μm, allowing normally-incident protons up to 12 MeV, He ions up to 46 MeV, Li up to 93 MeV and carbon up to 250 MeV to stop within its sensitive volume. A heavily boron doped diamond layer, about 1.5 μm thick, was grown on the *E* detector surface by Microwave Plasma Enhanced CVD (MWPE-CVD). The boron concentration was estimated by Hall effect measurements to be around $0.5 \bullet 10^{20} cm^{-3}$. Such B-doped diamond film is called dead layer (DL) from now on in the text. Then, a high quality intrinsic single crystal diamond film with a thickness of approximately 3 μm was selectively grown on the DL by MWPE-CVD, using a patterned chromium plasma-resistant mask. Such thin CVD diamond film was used as the sensitive volume for the *ΔE* detector. Finally, using the thermal evaporation technique, both CVD diamond surfaces were coated with 100 nm thick chromium Schottky contacts, that were vertically aligned with respect to each other. The metallic electrodes were circular-shaped, 500 μm and 700 μm in diameter for the *ΔE* and *E* detectors, respectively. The two detectors are based on CVD single crystal diamond in a p + -type/intrinsic/metal (p-i-m) configuration.

A custom PCB package with SMA connectors has been fabricated to mount the telescope detector while enabling microwire bonding on the top and on the bottom Cr contacts (of the *ΔE* and *E* detectors, respectively). The microwires connected the two electrodes to their dedicated electric tracks on the PCB. The B-doped diamond film was instead connected to its track by using silver paint. The detectors were reverse biased with a positive voltage applied on the Schottky contacts while the B-doped diamond common electrode was grounded. The adopted operational bias voltages were 10 V and 350 V for the *ΔE* and *E* detectors, respectively.

An optical picture of the *ΔE-E* telescope detector after packaging is shown in Fig. 1 a), while a schematic cross section of the device is shown in Fig. 1 b).

2.2. Experimental set-up description

The detector was characterised at the ion microprobe line of the Ruđer Bošković Institute (RBI) in Zagreb (Jakšić et al., 2007), using ion beams from the 6.0 MV Tandem Van der Graaff (High Voltage) and 1.0 MV Tandetron accelerator. The ion microprobe endstation (Fig. 1 c) is equipped with a magnetic quadrupole lens and a magnetic scanner unit capable of focusing the beam to approximately 1 μm in diameter and raster scanning the microbeam on the detector surface. In this way, spatially resolved information about the beam interaction with the detector is obtained, with resolution directly proportional to the beam spot size. The microbeam ion current was set below 1 fA (low current operation mode) to obtain a beam rate of about 1 kcps.

The diamond telescope was fixed on a sample holder, whose tilt angle could be controlled in order to change the angle of incidence of the particles with respect to the detector surface, and placed inside the vacuum chamber of the micro-beam line. To ensure the correct operation of the telescope, the detector was placed for the ions to imping onto the *ΔE* detector. The Ion Beam Induced Charge (IBIC) characterization was performed to study the detector response in terms of its charge collection properties and uniformity of the response with different ion species at different energies, as reported in Table 1. The uncertainty of the ion beam energy was 0.5%. The penetration depth in diamond of the ions used in the experiments ranges between 4.6 μm and 35.4 μm. This allows the ions to cross the *ΔE* stage and to stop in the *E* detector. The values of LET in diamond of the tested particles at the entrance of the detector, estimated by SRIM tables (Ziegler et al., 2010), vary between 170 keV/μm and 3139 keV/μm.

Two analogous conventional amplification chains, based on charge sensitive preamplifiers (Ortec 142) and shaping amplifiers (ORTEC 570), were used for the two telescope stages. The shaping time of the amplifier was set to 3 μs to optimise pile-up and noise. Pulse height spectra (PHS) for the incident ions were measured using a CANBERRA 8075 ADC connected to the computer. The gain of the shaping amplifier was modified for the different ions and energies to optimise the acquisition dynamic range.

The data acquisition of IBIC measurements was carried out by the software Spector (Cosic et al., 2019). During the raster scan irradiation, each event processed by the data acquisition corresponded to a single ion impinging on the detector. The system correlated and recorded the beam position (as (x,y) coordinates), pulse amplitude (proportional to the energy deposited in the detector) as well as the time-stamp of the event occurrence. To have separate IBIC measurements for both the *ΔE* and *E* detectors, all these data were acquired independently for the two stages. The data were then coupled in post-processing by looking for the

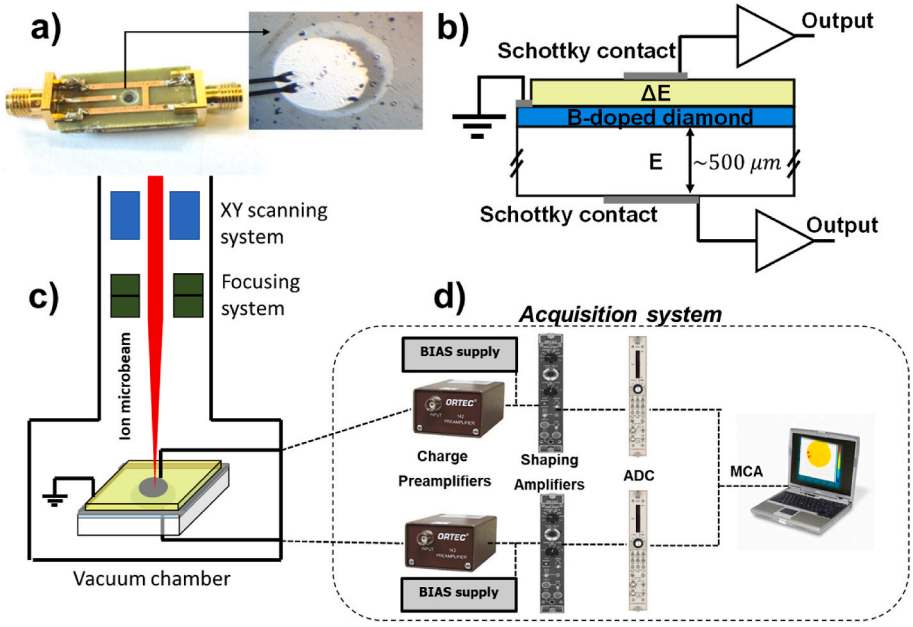

Fig. 1. a) Optical image of ΔE-E telescope detector; b) schematic cross section of the device; c) scheme of the IBIC setup; d) spectroscopic acquisition chain used in the experiment.

Table 1
Penetration depth and LET in diamond for the energy and type of ions employed in the experiment. Data taken from SRIM tables(Ziegler et al., 2010).

Ion type	Ion Energy (MeV)	Range in diamond (μm)	LET (keV/μm)
^{4}He	2.5	4.6	440
^{4}He	5	11.8	284
^{4}He	7.5	22.1	212
^{4}He	10	35.4	170
^{7}Li	4.86	4.9	880
^{7}Li	6.6	7	741
^{7}Li	10.3	12.8	562
^{7}Li	10.9	13.9	514
^{7}Li	14.8	21.9	441
^{12}C	11.3	5.1	2149
^{12}C	13.3	6	2030
^{12}C	16.67	7.8	1854
^{12}C	17.7	8.3	1806
^{12}C	20.8	10.1	1676
^{12}C	24	12.1	1563
^{16}O	15.6	5	3139
^{16}O	18	5.9	3011
^{16}O	22.5	7.4	2796

time coincidence between events in the two stages.

The energy calibration of the two electronic chains was carried out by using the combination of a precision pulse generator and of a silicon surface barrier detector (STIM) with known Charge Collection Efficiency (CCE) of 100%. The calibration for the diamond detector was then obtained by considering the mean energy needed to create an electron hole pair in silicon (3.6 eV) and in diamond (13.2 eV).

The uncertainty values reported for the deposited energy data shown in this paper were estimated considering only the statistical uncertainty (type-A). This was calculated by fitting the energy deposition distribution with a Gaussian curve whose mean value and standard deviation gave, respectively, the mean deposited energy and its standard uncertainty.

2.3. Geant4 Monte Carlo simulation

Monte Carlo simulations were carried out by means of Geant4 (Agostinelli et al., 2003; Allison et al., 2006, 2016), to support the experimental characterisation of the diamond telescope detector. The telescope structure represented in Fig. 1b was reproduced, creating two independent scoring volumes to simulate both ΔE and E stages. To optimise computational time, a low-energy production threshold was set on secondary electrons. This is done in Geant4 by defining the so called "production cut". The production-cut is the length for which, if a secondary is generated with such an energy that its range is lower than the production-cut, it will not be simulated and all its energy will be considered deposited within the volume it was generated in. Since most of the energy lost by the primary is deposited via secondary electrons, when simulating the ΔE, with a finite micrometric sensitive volume, we are interested in looking at those electrons getting out of the sensitive volume and therefore depositing only a fraction of their kinetic energy into it. The lower is the production-cut, the more accurate is therefore the simulation but the longer computational time is required. Setting an appropriate production-cut is fundamental to achieve a good accuracy while avoiding unnecessary computational efforts. As already successfully implemented by different authors for similar simulation conditions (Bolst et al., 2020; G Parisi et al., 2022), therefore, two regions were defined in the simulated geometry: a high precision region surrounding the detector with the minimum production-cut allowed by the physics used (250 eV in any material), and a low precision region all around with a higher cut set to 100 μm (corresponding to an energy cut of 167.252 keV for secondary electrons in diamond). To assure the simulation of any secondary that could hit the detectors, the high precision region was made to extend from each side of the detectors by the length of production-cut in the lower precision region (i.e. 100 μm).

From each scoring volume, the energy deposited in the volume, the path travelled by the particle depositing energy and the particle atomic number are scored together with an event ID. The number of the history simulated (an integer number increasing for each new primary particle simulated out of the simulation source) was chosen as event ID to univocally identify each event correlated to the same primary particle. While the deposited energy allows to obtain the energy deposition spectra in the two stages, the event ID is used to couple events between the two stages and the particle atomic number to identify the particle depositing energy.

3. Results and discussion

The IBIC maps, acquired by the *ΔE-E* telescope detector when the detector surface was raster scanned by a 24 MeV C ion beam, are depicted in Fig. 2 and Fig. 3. The maps display a representation of the average energy detected per pixel by the two detectors. The colours, from blue to red, represent the median energies per pixel, while white pixels indicate that no event has been detected at that position (signal below noise threshold). A good spatial resolution was achieved by the IBIC measurements, showing a well-defined sensitive volume (SV) for the *ΔE*, as shown in Fig. 2. No charge was collected outside the SV. Standard microscopic calibration grid was used to spatially calibrate the beam scanner before the experiment, allowing to measure the distances in the IBIC maps. The diameter of the SV of *ΔE* was estimated to be around 510 μm, in agreement with the nominal diameter size of the metallic electrode. The X and Y profiles of the IBIC map are also reported in Figs. 2 and 3 showing a quite constant signal inside the SV and it reduces drastically as the beam is outside the metallic contact for the *ΔE* stage, demonstrating a high transverse definition capability of the *ΔE* detector. As it can be observed in Fig. 3, the *E* detector size looked slightly larger than expected and the circular shape of the electrode (i.e. 800 μm in diameter) was not completely conserved. This is the result of a broadening of the electric field generated by the bias voltage, responsible for the charge collection. The p-i-m junction, indeed, depletes from the metal back-end electrode up to the p + common layer and, given the thickness of the detector, a broadening of the electric field lines towards the final part of the depletion region was expected. Since the telescope is meant to work in time-coincidence between the two stages, however, this broadening effect does not affect the final result as the effective SV of the E stage lays beneath the ΔE (since all the events in time coincidence seen by the E sit in correspondence of the ΔE above). The Al wires bonding spots (25 μm in diameter) are also clearly visible in Figs. 2 and 3. In particular, the carbon ions impinging on the wire bonding area deposits a higher energy in the ΔE layer and a lower one in the *E* stage, while the Al wires fully stop the ions before entering in the diamond SV.

The energy spectra, plotted in the upper part of Figs. 2 and 3, represent the pulse-heights distribution for all events detected from the full area scanned by 24 MeV of carbon ion as shown in the IBIC maps. These energy spectra include the area inside and outside the SV as well as its edges. The deposited energy distribution peak is well defined for both detectors. After fitting with a Gaussian function, it corresponds to an energy of 4.20 ± 0.28 MeV and 18.1 ± 1.4 MeV for the *ΔE* and *E* detector, respectively. A good homogeneity of the *ΔE* response was found for all the ions and energies investigated. The measured deposited energy, indeed, varied of about 7% its mean value throughout the whole sensitive area. This can be observed by looking either at the IBIC map shown in Fig. 2 and in the upper graph of Fig. 4, obtained by raster-scanning a Helium microbeam of 2.5 MeV over the surface of the detector. The E detector, instead, responded differently, as observed in the IBIC maps in Fig. 3 and in the lower graph of Fig. 4. Charge collection was less homogeneous than what found for *ΔE* and, more importantly, a region with a consistently lower CCE was observed at higher stopping power (Fig. 4). This lower CCE region in the E stage is found exactly in correspondence of the *ΔE* sensitive volume above, creating a sort of shadow on the E sensitive volume. The effect observed is most likely the result of a cross-talk between the two stages.

To characterise such cross-talk, the E detector's IBIC maps measured with different ions and energies have been analysed separating the part of the energy spectrum collected within the shadow, ε_{E_in}, and the complementary part of the spectrum collected outside, ε_{E_out}. The ratio between the two energies was then studied as a function of the ratio between the energy deposited in the E stage and the energy deposited in the ΔE stage, $\frac{\varepsilon_{E\_in}}{\varepsilon_{\Delta E}}$. As it could be observed in Fig. 5, the cross-talk effect was significant only when $\frac{\varepsilon_{E\_in}}{\varepsilon_{\Delta E}} < 1$. Such small ratio occurs when the energy deposited in the ΔE stage is very high and the energy deposited in the E stage is very low, i.e. for particles penetrating only few micrometres into the E stage. These particles, impinging at very low energy and thus very high LET values, lose a non-negligible amount of their energy crossing the thin front-electrode (about 100 nm thick) that defines the ΔE sensitive volume. So, in correspondence of the ΔE, those particles get to the E stage with lower energy than all around and deposit therefore less energy. However, the energy lost in the front-electrode is

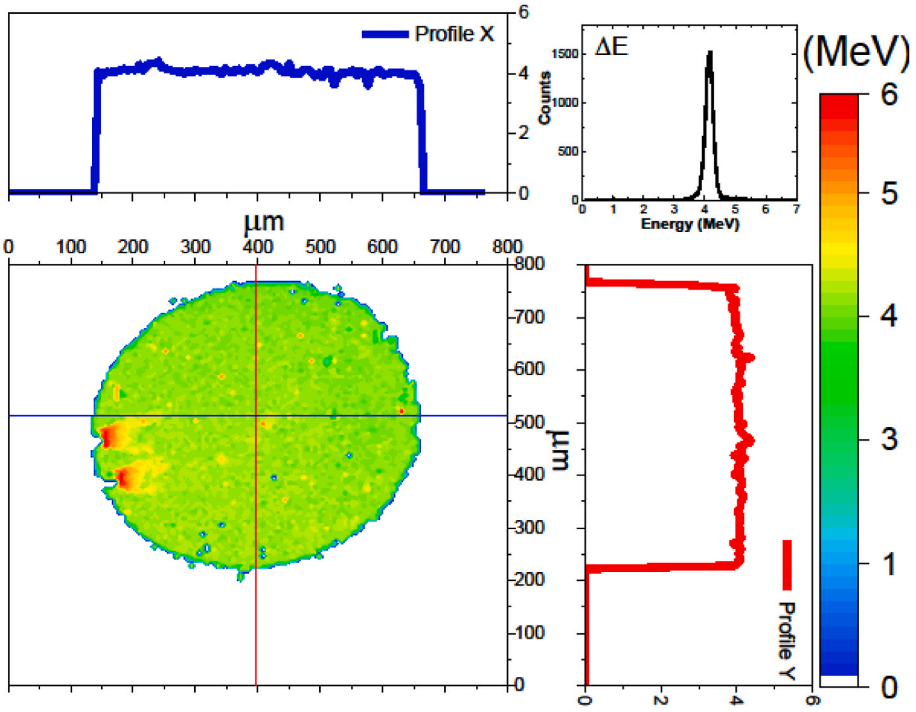

Fig. 2. Measured IBIC map obtained by raster scanning with 24 MeV carbon ions the whole surface of ΔE detector. The X and Y profiles of the sensitive area and relative energy spectra are also shown.

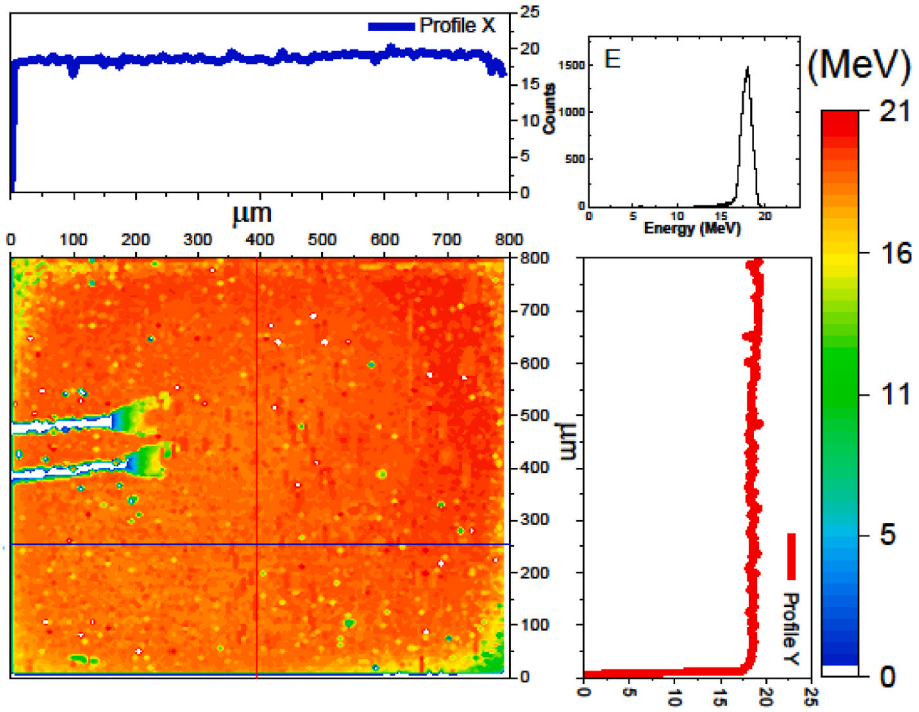

Fig. 3. Measured IBIC map of E detector. The X and Y profiles of the sensitive area and relative energy spectra are also shown.

not enough to explain the low ratios observed and a cross-talk has to be assumed to fully explain the effect. The reasons behind this cross-talk are still under investigation, but it is currently thought to be the consequence of the non-zero resistance in the DL, which is a known issue of monolithic solid-state telescopes (Kordyasz et al., 2006; Zhu et al., 2021). When a very high pulse is generated in one of the two stages, a non-negligible current would flow across the DL generating a potential difference affecting the amplitude of the smaller signal in the other stage. A similar effect is therefore expected to affect also the ΔE stage, in case the energy deposited in the ΔE is very small and the energy deposited in the E is very high, i.e. for particles penetrating deep into the E stage and stopping around its back-end. However, with the experimental data collected for this work we are not able to verify and quantify this. Future works will be dedicated to detailed investigation of this effect and its reduction.

To deal with the cross-talk, a correction method that could be generally used in any application of the telescope was developed. To this purpose, the data plotted in Fig. 5 were well fitted with an exponential function $f_C\left(\frac{\varepsilon_{E\_in}}{\varepsilon_{\Delta E}}\right)$:

$$\frac{\varepsilon_{E\_in}}{\varepsilon_{E\_out}} = f_C\left(\frac{\varepsilon_{E\_in}}{\varepsilon_{\Delta E}}\right) = 1 - 0.49e^{-2.45\frac{\varepsilon_{E\_in}}{\varepsilon_{\Delta E}}}$$

Once the function was found by fitting the data collected during this work, it could be used to correct any future data-set. The data presented in this work were all successfully corrected for the cross-talk effect.

The lower graph of Fig. 6 shows the difference between the nominal beam energy and the corrected energy measured by the *E* as a function of the LET in diamond of the incident ion, estimated at its beam energy reduced of the energy measured by the *ΔE*. The energy thus calculated correspond to the energy deposited in a diamond film consisting of *ΔE* and DL. The upper graph of Fig. 6 shows the energy measured by the *ΔE* detector plotted against the nominal LET in diamond of the incident ion (as reported in Table 1). The different ions' LET values in diamond were estimated by SRIM tables (Ziegler et al., 2010). A good linearity of the response of both stages could be observed in Fig. 6 as given by fitting experimental data with linear function. As the *ΔE* stage measured the energy deposited in its sensitive volume by reasonably straight particle beams, a rough estimate of the *ΔE* thickness could be obtained by linear fitting the set of data in Fig. 6. The same could be done for the sum of *ΔE* and DL thicknesses. A thickness of $2.6 \pm 0.1\mu m$ and of $4 \pm 0.3\mu m$ was estimated, respectively, for the *ΔE* stage and for the sum of *ΔE* and DL, so that a thickness of $1.4 \pm 0.3\mu m$ can be calculated for DL. Such values reasonably agree with the nominal thicknesses of *ΔE* and DL.

To obtain a more accurate measurement of the *ΔE* and DL thicknesses, dedicated measurements were carried out with a 24 MeV carbon microbeam, tilting the detector at several increasing angles θ with respect to the beam direction. The Bragg curve of 24 MeV carbon ions in diamond was first calculated by the nuclear simulation program SRIM and then it was fitted by the equation $\frac{Ae^{Bx}+Ce^{Dx}}{1+Ee^{Fx}}$, where x is the penetration depth along the direction of propagation of the impinging particle. The six parameters, i.e. A, B, C, D and F, was thus calculated from the best fit of the data as reported in Fig. 7. By neglecting straggling effects, the distance travelled by the impinging ions within the diamond layer is $\frac{d}{\cos(\theta)}$, where d is the sensitive region thickness, which need to be calculated. The energy deposited in diamond as a function of the tilting angle, $E(\theta)$, can be calculated by the Bragg curve function integrated between 0 and $\frac{d}{\cos(\theta)}$. This energy was estimated at several thicknesses with a d = 0.1 μm increase between each other and compared with the measured data.

The measured energy deposited in *ΔE* stage by 24 MeV carbon ions as a function of the tilting angle θ is reported in the upper level of Fig. 8. While the difference between the nominal beam energy and the energy measured by the *E* stage as a function of θ is reported in the lower laver of Fig. 8. A systematic error in the tilt-angle data was observed and opportunely corrected for by considering an offset of 11°. The thicknesses of the *ΔE* and DL layers were calculated through an iterative procedure finding the thickness that gives the best matching between the energy deposition measured and that calculated $E(\theta)$ at different angles. The best matching between the integral curve and the measured points, according to the R^2 value, was found to be $2.5 \pm 0.1\mu m$ for the *ΔE* and $4.3 \pm 0.1\mu m$ for the sum of *ΔE* and DL (so $1.8 \pm 0.1\mu m$ thick DL), as shown by Fig. 8. These thicknesses are compatible with those previously estimated (see Fig. 6).

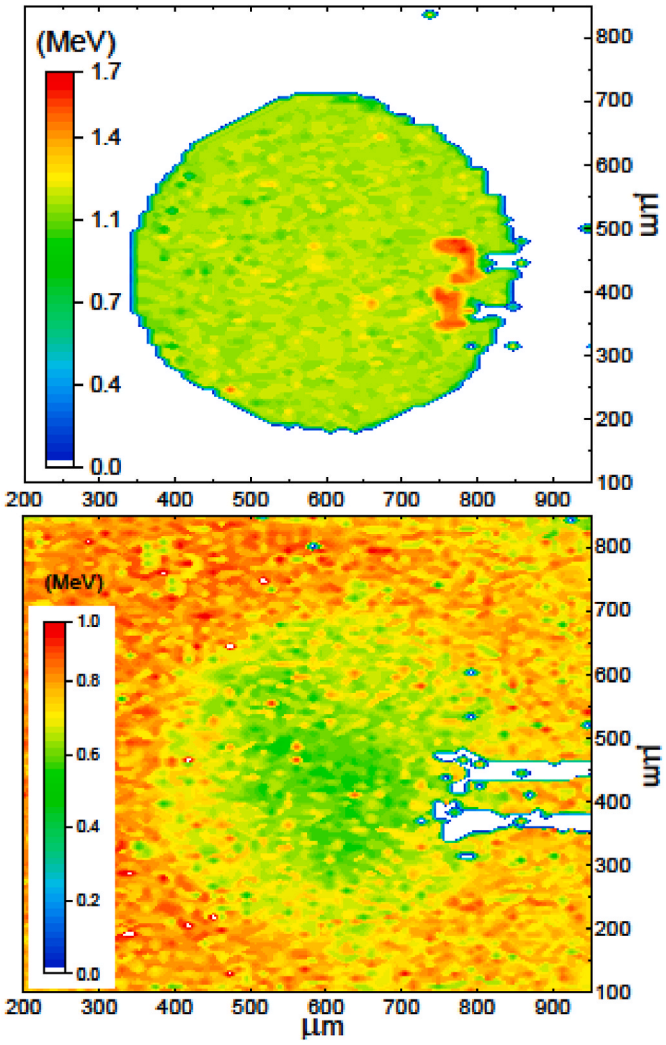

Fig. 4. IBIC maps collected by ΔE (upper level) and E (lower level) irradiated with 2.5 MeV He microbeam.

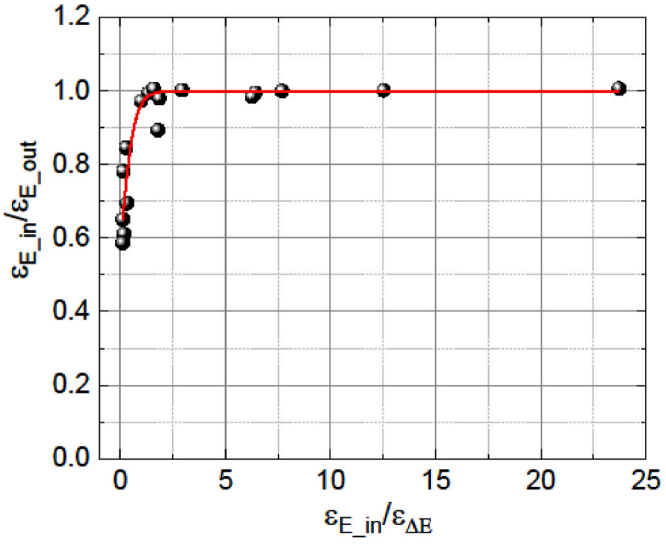

Fig. 5. Ratio between the energy deposited by different ions in the E stage inside and outside the shadow as a function of the ratio between the energy deposited in the E stage inside the shadow and the energy deposited in the ΔE.

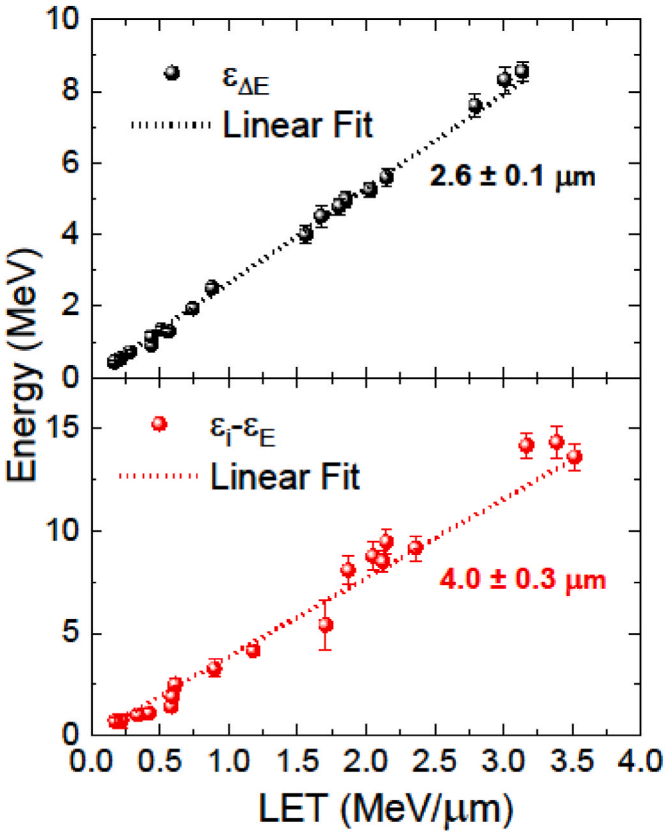

Fig. 6. a) The energy measured by ΔE detector as a function of the LET in diamond of the ions employed in this experiment. B) Difference between nominal energy of impinging ions and energy measure by E detector as a function of the LET in diamond of incident particles considering the energy lost in ΔE stage. Linear fits of the experimental data are also reported in the figure as dashed lines.

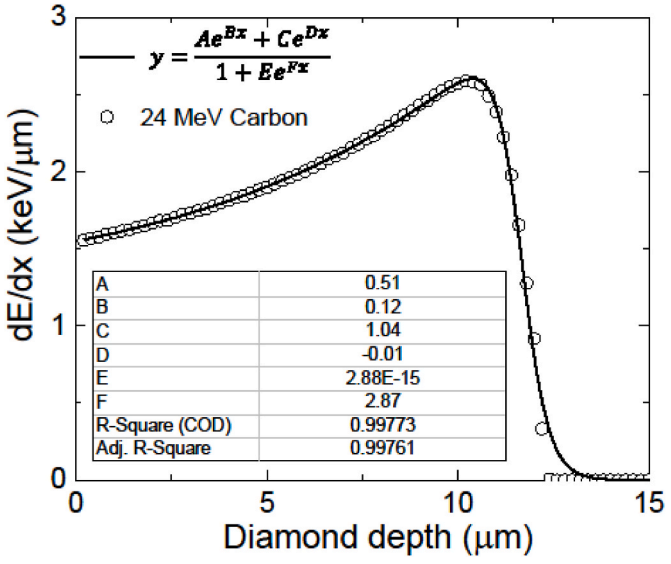

Fig. 7. Bragg curve of 24 MeV carbon in diamond simulated by SRIM (Ziegler et al., 2010). Fitting curve of the empirical equation reported in the text is also shown in figure.

The thickness uncertainty reported is taken from the uncertainty of the fit, when considering the uncertainty of the deposited energy (type-A), of the tilt-angle (type-B) and of the ion beam energy (type-B). The

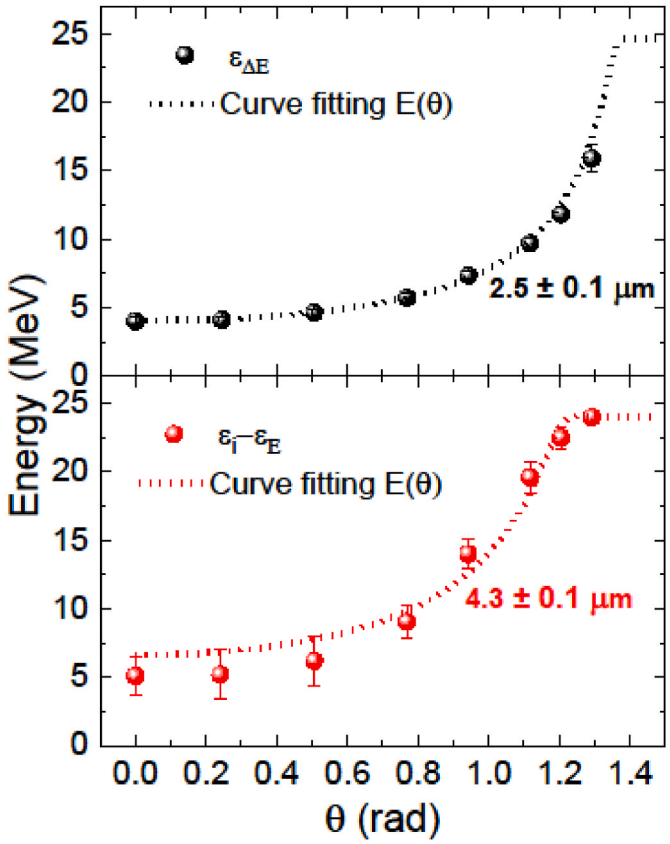

Fig. 8. Experimental values of energy loss of alpha particle in the diamond active layer as a function of incidence angle. Theoretical curve E (θ) is also reported as dashed line.

uncertainties of the tilt-angle (0.009 rad) and of the ion beam energy (0.5%), being very small, could not be observed neither in Fig. 6 nor in Fig. 8. The thicknesses found by this experiment are used to properly model the detector in the Geant4 code, as described in the Geant4 Monte Carlo simulation section.

Fig. 9 shows different spectra collected by the two stages irradiating the telescope on a subregion of the order of $10^4 \mu m^2$ within the ΔE's SV with Helium, Lithium and Carbon ions at different energies. The spectra were generated considering events in time coincidence between the two stages. As expected, for higher nominal beam energy the spectra collected by the ΔE, behaving like a microdosimeter and hence measuring the energy deposited along its thickness, moved towards lower energies while the spectra collected by the E, measuring the residual energy of the particle, moved towards higher energies. The simulated spectra resulting from the Geant4 Monte Carlo simulations are also reported in Fig. 9 as dashed lines. Even if small discrepancies in the deposited energy distribution position and broadening were sometimes observed for some of the measured points (for instance 2.5 MeV He and 4.86 MeV Li in Fig. 9), the overall agreement between measured and simulated spectra proved the capability of the simulation code to reproduce, within the thickness's uncertainty, the energy deposition spectra measured by the telescope.

The fundamental feature of telescope detectors is the scatter plot, where all the events measured in coincidence are plotted in a $\varepsilon_{\Delta E}$ vs ε_E graph, with ε_x being the energy deposited in stage x. The scatter plot is unique for each telescope detector (it depends indeed on its characteristics, for instance the thickness of ΔE, DL and E) and allows to discriminate the type of particle depositing energy. The pair of events in coincidence ($\varepsilon_{\Delta E}$, ε_E) would indeed lay in a specific region of the scatter plot according to the type of particle. Geant4 Monte Carlo simulations of the ions studied during this experimental campaign (He, Li, C and O) were carried out considering a range of energy from 0 to 30 MeV of used ions as well as the telescope geometry and the above estimated diamond layer thicknesses (i.e. ΔE and DL). The resulting scatter plot is shown in Fig. 10, together with the scatter plot of the different experimental points measured. Results from measurements sit well within the simulated curve, which are well defined and separated from one another. Hence, the telescope potential as a particle discriminator is here proved.

4. Conclusions

A novel diamond-based telescope detector has been thoroughly characterised at very low energies ions microbeam (less than 30 MeV) by means of IBIC technique at the Ruder Boskovic Institute (RBI), Zagreb, Croatia. The detector is made up of 2 monolithic stages: a thin front stage 2.5 μm thick, the ΔE, and a thicker stage 500 μm thick, the E. The thicknesses of the two stages can be optimised according to the specific application of the telescope. The two stages share a common ground contact consisting of a boron doped diamond layer, DL.

Measurements carried out with the same beam condition changing the detector tilt angle with respect of the beam direction, allowed to

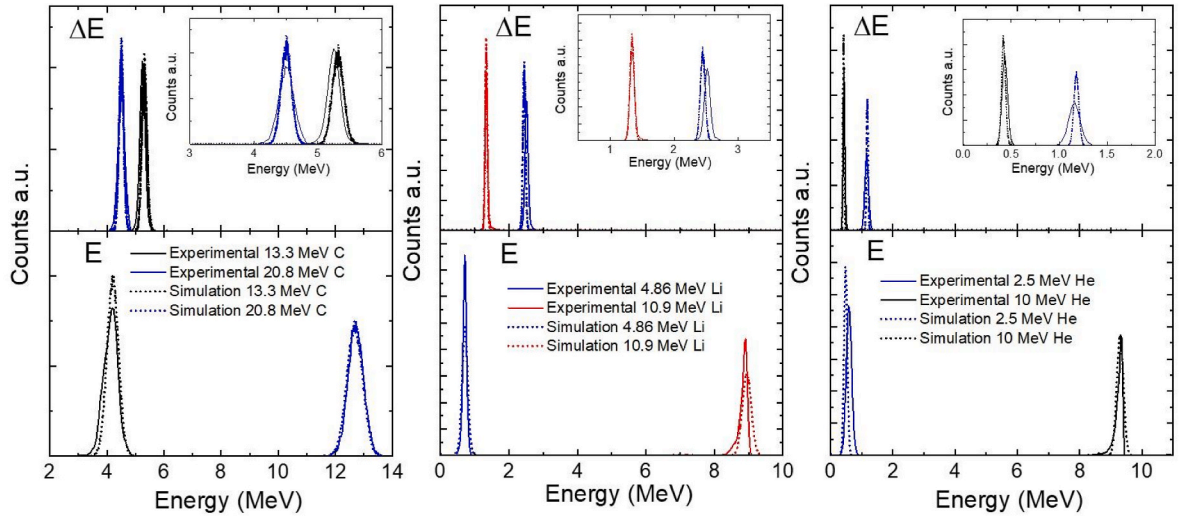

Fig. 9. Experimental (solid lines) and simulated (dashed lines) spectra in coincidence mode from the ΔE and E detectors measured with Carbon, Lithium and Helium ions of different energies.

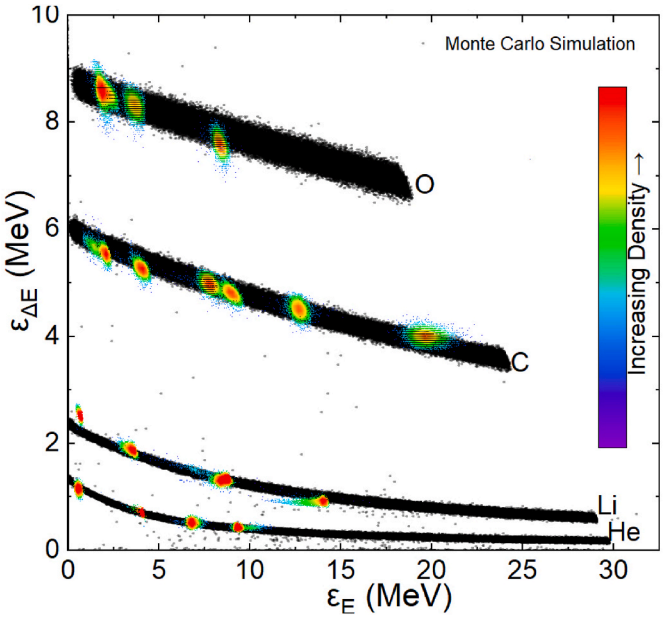

Fig. 10. ΔE-E scatter plot density acquired by the diamond telescope with the for different ions and energies. Monte Carlo simulations considering the telescope geometry is also reported in the figure as black dots.

accurately estimate the thicknesses of ΔE and of the Boron doped diamond dead-layer shared between the two stages. The thickness of the ΔE and of the DL turned out to be $2.5 \pm 0.1\ \mu m$ and $1.8 \pm 0.1\ \mu m$, respectively.

IBIC analysis was carried out with He, Li, C and O ions at different low energies. The telescope proved to be a reliable detector, with well confined ΔE sensitive volume whose response showed an excellent homogeneity of about 7% throughout the whole sensitive area. A good linearity with the LET in diamond of incident ions was obtained in the whole investigated LET range (170–3139 keV/μm), indicating the telescope potential to be used as a microdosimeter and as a LET counter.

However, a cross-talk effect was observed for ions depositing a higher energy in the ΔE stage than in the E stage. The cross-talk manifested as a diminished charge collection efficiency (CCE) of the E stage in the region beneath the ΔE. A correction function was implemented and successfully used to correct the energy measured by the E for the cross-talk. The effect was probably related to the non-zero resistance of the DL. However, the origin of the cross-talk is still under investigation. Future development of the diamond telescope technology will involve a detailed investigation of such cross-talk effect and its improvement.

A general good agreement between the experimental and simulated spectra in coincidence mode measured from the ΔE and E detectors of the telescope was observed for all tested ions. The scatter plot resulting from the combination of simulations and measured data, gave a proof of concept for the diamond telescope to be used as a particle discriminator. This work also gave confidence to the use of the Geant4 code implemented to simulate the diamond telescope. A dedicated work to fully validate the code is foreseen.

A characterisation of the telescope performances under medium and high energy ion beams is foreseen. Its capability as a particle discriminator in unknown mixed radiation fields, such as those found in nuclear physics experiments, will be assessed and a reliable discrimination method will be implemented. Future works will also include the application of the telescope to clinical hadron therapy beams, where it will be used simultaneously as a microdosimeter and as a particle discriminator.

Authors CRediT contributor roles

Claudio Verona: Conceptualization (lead) Data curation (equal) Formal analysis (lead) Funding acquisition (lead) Investigation (lead) Methodology (lead) Project administration (lead) Supervision (equal) Visualization (equal) Writing - original draft (lead) Writing - review & editing (lead) Gabriele Parisi: Conceptualization (equal) Data curation (lead) Formal analysis (lead) Investigation (lead) Methodology (lead) Software (lead) Visualization (equal) Writing - original draft (lead) Writing - review & editing (lead) Silvia Cesaroni: Methodology (supporting) Andreo Crnjac: Investigation (supporting) Resources (equal) Software (supporting) Writing - review & editing (equal) Milko Jaksic: Investigation (supporting) Resources (equal) Software (supporting) Writing - review & editing (equal) Marco Marinelli: Supervision (equal) Silvia Palomba: Formal analysis (supporting) Investigation (lead) Francesco Romano: Conceptualization (supporting) Supervision (equal) Giuseppe Schettino: Conceptualization (supporting) Supervision (equal) Writing - review & editing (equal) Gianluca Verona Rinati: Conceptualization (equal) Investigation (equal) Methodology (equal) Supervision (equal) Writing - original draft (supporting) Writing - review & editing (equal)Writing - review & editing (equal)

Declaration of competing interest

The authors declare that they have no known competing financial interests or personal relationships that could have appeared to influence the work reported in this paper.

Data availability

The data that has been used is confidential.

Acknowledgement

The research leading to this result has been supported by the RADIATE project under the Grant Agreement 824096 from the EU Research and Innovation programme HORIZON 2020, and by EPSRC industrial CASE award.

References

Agosteo, S., Borsato, E., Corso, F.D., Fazzi, A., Gonella, F., Introini, M.V., Lorenzoli, M., Pegoraro, M., Pola, A., Varoli, V., Zotto, P., 2014. Study of the direct response of a monolithic silicon telescope to charged particles at different energies. Prog. Nucl. Sci. Technol. 4, 717–720. https://doi.org/10.15669/pnst.4.717.

Agosteo, S., Fallica, P.G., Fazzi, A., Introini, M.V., Pola, A., Valvo, G., 2008. A pixelated silicon telescope for solid state microdosimetry. Radiat. Meas. 43, 585–589. https://doi.org/10.1016/j.radmeas.2007.12.053.

Agostinelli, S., Allison, J., Amako, K., Apostolakis, J., Araujo, H., Arce, P., Asai, M., Axen, D., Banerjee, S., Barrand, G., Behner, F., Bellagamba, L., Boudreau, J., Broglia, L., Brunengo, A., Burkhardt, H., Chauvie, S., Chuma, J., Chytracek, R., Cooperman, G., Cosmo, G., Degtyarenko, P., Dell'Acqua, A., Depaola, G., Dietrich, D., Enami, R., Feliciello, A., Ferguson, C., Fesefeldt, H., Folger, G., Foppiano, F., Forti, A., Garelli, S., Giani, S., Giannitrapani, R., Gibin, D., Gómez Cadenas, J.J., González, I., Gracia Abril, G., Greeniaus, G., Greiner, W., Grichine, V., Grossheim, A., Guatelli, S., Gumplinger, P., Hamatsu, R., Hashimoto, K., Hasui, H., Heikkinen, A., Howard, A., Ivanchenko, V., Johnson, A., Jones, F.W., Kallenbach, J., Kanaya, N., Kawabata, M., Kawabata, Y., Kawaguti, M., Kelner, S., Kent, P., Kimura, A., Kodama, T., Kokoulin, R., Kossov, M., Kurashige, H., Lamanna, E., Lampén, T., Lara, V., Lefebure, V., Lei, F., Liendl, M., Lockman, W., Longo, F., Magni, S., Maire, M., Medernach, E., Minamimoto, K., Mora de Freitas, P., Morita, Y., Murakami, K., Nagamatu, M., Nartallo, R., Nieminen, P., Nishimura, T., Ohtsubo, K., Okamura, M., O'Neale, S., Oohata, Y., Paech, K., Perl, J., Pfeiffer, A., Pia, M.G., Ranjard, F., Rybin, A., Sadilov, S., Di Salvo, E., Santin, G., Sasaki, T., Savvas, N., Sawada, Y., Scherer, S., Sei, S., Sirotenko, V., Smith, D., Starkov, N., Stoecker, H., Sulkimo, J., Takahata, M., Tanaka, S., Tcherniaev, E., Safai Tehrani, E., Tropeano, M., Truscott, P., Uno, H., Urban, L., Urban, P., Verderi, M., Walkden, A., Wander, W., Weber, H., Wellisch, J.P., Wenaus, T., Williams, D.C., Wright, D., Yamada, T., Yoshida, H., Zschiesche, D., 2003. Geant4—a simulation toolkit. Nucl. Instruments Methods Phys. Res. Sect. A Accel. Spectrometers, Detect. Assoc. Equip. 506, 250–303. https://doi.org/10.1016/s0168-9002(03)01368-8.

Ahmadov, G.S., Kopatch, Y.N., Telezhnikov, S.A., Ahmadov, F.I., Granja, C., Garibov, A. A., Pospisil, S., 2015. Detection of ternary and quaternary fission fragments from 252Cf with a position-sensitive ΔE-E telescope based on silicon detectors. Phys. Part. Nucl. Lett. 12, 542–549. https://doi.org/10.1134/s1547477115040032.

Allison, J., Amako, K., Apostolakis, J., Araujo, H., Arce Dubois, P., Asai, M., Barrand, G., Capra, R., Chauvie, S., Chytracek, R., Cirrone, G.A.P., Cooperman, G., Cosmo, G.,

Cuttone, G., Daquino, G.G., Donszelmann, M., Dressel, M., Folger, G., Foppiano, F., Generowicz, J., Grichine, V., Guatelli, S., Gumplinger, P., Heikkinen, A., Hrivnacova, I., Howard, A., Incerti, S., Ivanchenko, V., Johnson, T., Jones, F., Koi, T., Kokoulin, R., Kossov, M., Kurashige, H., Lara, V., Larsson, S., Lei, F., Link, O., Longo, F., Maire, M., Mantero, A., Mascialino, B., McLaren, I., Mendez Lorenzo, P., Minamimoto, K., Murakami, K., Nieminen, P., Pandola, L., Parlati, S., Peralta, L., Perl, J., Pfeiffer, A., Pia, M.G., Ribon, A., Rodrigues, P., Russo, G., Sadilov, S., Santin, G., Sasaki, T., Smith, D., Starkov, N., Tanaka, S., Tcherniaev, E., Tome, B., Trindade, A., Truscott, P., Urban, L., Verderi, M., Walkden, A., Wellisch, J.P., Williams, D.C., Wright, D., Yoshida, H., 2006. Geant4 developments and applications. IEEE Trans. Nucl. Sci. 53, 270–278. https://doi.org/10.1109/tns.2006.869826.

Allison, J., Amako, K., Apostolakis, J., Arce, P., Asai, M., Aso, T., Bagli, E., Bagulya, A., Banerjee, S., Barrand, G., Beck, B.R., Bogdanov, A.G., Brandt, D., Brown, J.M.C., Burkhardt, H., Canal, P., Cano-Ott, D., Chauvie, S., Cho, K., Cirrone, G.A.P., Cooperman, G., Cortés-Giraldo, M.A., Cosmo, G., Cuttone, G., Depaola, G., Desorgher, L., Dong, X., Dotti, A., Elvira, V.D., Folger, G., Francis, Z., Galoyan, A., Garnier, L., Gayer, M., Genser, K.L., Grichine, V.M., Guatelli, S., Guèye, P., Gumplinger, P., Howard, A.S., Hřivnáčová, I., Hwang, S., Incerti, S., Ivanchenko, A., Ivanchenko, V.N., Jones, F.W., Jun, S.Y., Kaitaniemi, P., Karakatsanis, N., Karamitros, M., Kelsey, M., Kimura, A., Koi, T., Kurashige, H., Lechner, A., Lee, S.B., Longo, F., Maire, M., Mancusi, D., Mantero, A., Mendoza, E., Morgan, B., Murakami, K., Nikitina, T., Pandola, L., Paprocki, P., Perl, J., Petrović, I., Pia, M.G., Pokorski, W., Quesada, J.M., Raine, M., Reis, M.A., Ribon, A., Ristić Fira, A., Romano, F., Russo, G., Santin, G., Sasaki, T., Sawkey, D., Shin, J.I., Strakovsky, I.I., Taborda, A., Tanaka, S., Tomé, B., Toshito, T., Tran, H.N., Truscott, P.R., Urban, L., Uzhinsky, V., Verbeke, J.M., Verderi, M., Wendt, B.L., Wenzel, H., Wright, D.H., Wright, D.M., Yamashita, T., Yarba, J., Yoshida, H., 2016. Recent developments in Geant4. Nucl. Instruments Methods Phys. Res. Sect. A Accel. Spectrometers, Detect. Assoc. Equip. 835, 186–225. https://doi.org/10.1016/j.nima.2016.06.125.

Bolst, D., Guatelli, S., Tran, L.T., Rosenfeld, A.B., 2020. The impact of sensitive volume thickness for silicon on insulator microdosimeters in hadron therapy. Phys. Med. Biol. 65, 35004 https://doi.org/10.1088/1361-6560/ab623f.

Carboni, S., Barlini, S., Bardelli, L., Le Neindre, N., Bini, M., Borderie, B., Bougault, R., Casini, G., Edelbruck, P., Olmi, A., Pasquali, G., Poggi, G., Rivet, M.F., Stefanini, A. A., Baiocco, G., Berjillos, R., Bonnet, E., Bruno, M., Chbihi, A., Cruceru, I., Degerlier, M., Dueñas, J.A., Galichet, E., Gramegna, F., Kordyasz, A., Kozik, T., Kravchuk, V.L., Lopez, O., Marchi, T., Martel, I., Morelli, L., Parlog, M., Petrascu, H., Rosato, E., Seredov, V., Vient, E., Vigilante, M., Alba, R., Santonocito, D., Maiolino, C., 2012. Particle identification using the technique and pulse shape discrimination with the silicon detectors of the FAZIA project. Nucl. Instruments Methods Phys. Res. Sect. A Accel. Spectrometers, Detect. Assoc. Equip. 664, 251–263. https://doi.org/10.1016/j.nima.2011.10.061.

Cesaroni, S., Marinelli, M., Milani, E., Prestopino, G., Verona, C., Verona-Rinati, G., 2019. ΔE-E single crystal diamond based telescope. Nucl. Instruments Methods Phys. Res. Sect. A Accel. Spectrometers, Detect. Assoc. Equip. 947 https://doi.org/10.1016/j.nima.2019.162744.

Ciampi, C., Pasquali, G., Altana, C., Bini, M., Boscardin, M., Calcagno, L., Casini, G., Cirrone, G.A.P., Fazzi, A., Giove, D., Gorini, G., Labate, L., La Via, F., Lanzalone, G., Litrico, G., Muoio, A., Ottanelli, P., Poggi, G., Puglia, S.M.R., Rebai, M., Ronchin, S., Santangelo, A., Stefanini, A.A., Trifirò, A., Tudisco, S., Zimbone, M., 2019. Nuclear fragment identification with ΔE-E telescopes exploiting silicon carbide detectors. Nucl. Instruments Methods Phys. Res. Sect. A Accel. Spectrometers, Detect. Assoc. Equip. 925, 60–69. https://doi.org/10.1016/j.nima.2019.01.085.

Cosic, D., Bogovac, M., Jaksic, M., 2019. Data acquisition and control system for an evolving nuclear microprobe. Nucl. Instruments Methods Phys. Res. Sect. B-Beam Interact. with Mater. Atoms 451, 122–126. https://doi.org/10.1016/j.nimb.2019.05.047.

Davis, J.A., Ganesan, K., Prokopovich, D.A., Petasecca, M., Lerch, M.L.F., Jamieson, D.N., Rosenfeld, A.B., 2017. A 3D lateral electrode structure for diamond based microdosimetry. Appl. Phys. Lett. 110 https://doi.org/10.1063/1.4973628.

de Boer, W., Bol, J., Furgeri, A., Müller, S., Sander, C., Berdermann, E., Pomorski, M., Huhtinen, M., 2007. Radiation hardness of diamond and silicon sensors compared. Phys. Status Solidi 204, 3004–3010. https://doi.org/10.1002/pssa.200776327.

Gabrysch, M., Majdi, S., Twitchen, D.J., Isberg, J., 2011. Electron and hole drift velocity in chemical vapor deposition diamond. J. Appl. Phys. 109 https://doi.org/10.1063/1.3554721.

Guan, F., Wang, Y., Diao, X., Qin, Y., Qin, Z., Guo, D., Wu, Q., Si, D., Xiao, S., Zhang, B., Zhang, Y., Zhao, X., Xiao, Z., 2022. Track recognition for the ΔE−E telescopes with silicon strip detectors. Nucl. Instruments Methods Phys. Res. Sect. A Accel. Spectrometers, Detect. Assoc. Equip. 1029 https://doi.org/10.1016/j.nima.2022.166461.

Gunzert-Marx, K., Iwase, H., Schardt, D., Simon, R.S., 2008. Secondary beam fragments produced by 200 MeV/u 12C ions in water and their dose contributions in carbon ion radiotherapy. New J. Phys. 10 https://doi.org/10.1088/1367-2630/10/7/075003.

Gunzert-Marx, K., Schardt, D., Simon, R.S., 2004. Fast neutrons produced by nuclear fragmentation in treatment irradiations with 12C beam. Radiat. Protect. Dosim. 110, 595–600. https://doi.org/10.1093/rpd/nch138.

Isberg, J., Hammersberg, J., Johansson, E., Wikstrom, T., Twitchen, D.J., Whitehead, A. J., Coe, S.E., Scarsbrook, G.A., 2002. High carrier mobility in single-crystal plasma-deposited diamond. Science 297, 1670–1672. https://doi.org/10.1126/science.1074374.

Jakšić, M., Bogdanović Radović, I., Bogovac, M., Desnica, V., Fazinić, S., Karlušić, M., Medunić, Z., Muto, H., Pastuović, Ž., Siketić, Z., Skukan, N., Tadić, T., 2007. New capabilities of the Zagreb ion microbeam system. Nucl. Instrum. Methods Phys. Res. Sect. B Beam Interact. Mater. Atoms 260, 114–118. https://doi.org/10.1016/j.nimb.2007.01.252.

Jin, S.L., Wang, J.S., Yang, Y.Y., Huang, M.R., Wang, Q., Han, J.L., Ma, P., Ma, J.B., Bai, Z., Chen, J.B., Li, Y., Jin, L., Zhao, M.H., Wada, R., 2013. A ΔE-E telescope array for radioactive beam experiments. Nucl. Instrum. Methods Phys. Res. Sect. B Beam Interact. Mater. Atoms 317, 728–730. https://doi.org/10.1016/j.nimb.2013.07.044.

Kordyasz, A.J., Iwanicki, J., Kowalczyk, M., Kulczycka, E., Nossarzewska-Orłowska, E., Lipiński, D., Brzozowski, A., 2006. Pulse-shape analysis of signals from monolithic silicon – telescopes produced by the quasi-selective epitaxy. Nucl. Instruments Methods Phys. Res. Sect. A Accel. Spectrometers, Detect. Assoc. Equip. 568, 778–783. https://doi.org/10.1016/j.nima.2006.08.145.

Kramer, M., Scifoni, E., Schuy, C., Rovituso, M., Tinganelli, W., Maier, A., Kaderka, R., Kraft-Weyrather, W., Brons, S., Tessonnier, T., Parodi, K., Durante, M., 2016. Helium ions for radiotherapy? Physical and biological verifications of a novel treatment modality. Med. Phys. 43, 1995. https://doi.org/10.1118/1.4944593.

Ma, N.-R., Lin, C.-J., Wang, J.-S., Yang, L., Wang, D.-X., Zheng, L., Xu, S.-W., Sun, L.-J., Jia, H.-M., Ma, J.-B., Ma, P., Jin, S.-L., Bai, Z., Yang, Y.-Y., Xu, X.-X., Zhang, G.-L., Yang, F., He, J.-J., Zhang, H.-Q., Liu, Z.-H., 2016. A multilayer Δ E - E R telescope for breakup reactions at energies around the Coulomb barrier. Chin. Phys. C 40. https://doi.org/10.1088/1674-1137/40/11/116004.

Matsufuji, N., Fukumura, A., Komori, M., Kanai, T., Kohno, T., 2003. Influence of fragment reaction of relativistic heavy charged particles on heavy-ion radiotherapy. Phys. Med. Biol. 48, 1605–1623. https://doi.org/10.1088/0031-9155/48/11/309.

Matsufuji, N., Komori, M., Sasaki, H., Akiu, K., Ogawa, M., Fukumura, A., Urakabe, E., Inaniwa, T., Nishio, T., Kohno, T., Kanai, T., 2005. Spatial fragment distribution from a therapeutic pencil-like carbon beam in water. Phys. Med. Biol. 50, 3393–3403. https://doi.org/10.1088/0031-9155/50/14/014.

Mazzucconi, D., Bortot, D., Pola, A., Fazzi, A., Cazzola, L., Conte, V., Cirrone, G.A.P., Petringa, G., Cuttone, G., Manti, L., Agosteo, S., 2021. Experimental investigation at CATANA facility of n-(10)B and p-(11)B reactions for the enhancement of proton therapy. Phys. Med. 89, 226–231. https://doi.org/10.1016/j.ejmp.2021.08.008.

Mitcuk, V.V., Mordovskoy, M.V., 2019. ΔE–E telescope for the detection of charged particles based on a Si detector and a SiPM array with scintillation crystals. Phys. At. Nucl. 81, 1471–1476. https://doi.org/10.1134/s1063778818100101.

Mueller, A.C., Bazin, D., Schmidt-Ott, W.D., Anne, R., Guerreau, D., Guillemaud-Mueller, D., Saint-Laurent, M.G., Borrel, V., Jacmart, J.C., Pougheon, F., Richard, A., 1988. ?-Delayed neutron emission of15B,18C,19,20N,34,35Al and39P. Zeitschrift fr Phys. A At. Nucl. 330, 63–68. https://doi.org/10.1007/bf01287265.

Parisi, Gabriele, Pola, A., Bortot, D., Mazzucconi, D., D'Angelo, G., Magni, C., Postuma, I., Bortolussi, S., Protti, N., Altieri, S., Tamburini, U.A., Vercesi, V., Agosteo, S., 2022a. Development of the ACSpect neutron spectrometer: technological advance and response against an accelerator-based neutron beam. Radiat. Meas. 154 https://doi.org/10.1016/j.radmeas.2022.106776.

Parisi, G., Schettino, G., Romano, F., 2022b. A systematic study of the contribution of counting statistics to the final lineal energy uncertainty in microdosimetry. Phys. Med. Biol. 67 https://doi.org/10.1088/1361-6560/ac79fb.

Pasquali, G., Pastore, G., Le Neindre, N., Ademard, G., Barlini, S., Bini, M., Bonnet, E., Borderie, B., Bougault, R., Casini, G., Chbihi, A., Cinausero, M., Dueñas, J.A., Edelbruck, P., Frankland, J.D., Gramegna, F., Gruyer, D., Kordyasz, A., Kozik, T., Lopez, O., Marchi, T., Morelli, L., Olmi, A., Ordine, A., Pârlog, M., Piantelli, S., Poggi, G., Rivet, M.F., Rosato, E., Salomon, F., Spadaccini, G., Stefanini, A.A., Valdrè, S., Vient, E., Twaróg, T., Alba, R., Maiolino, C., Santonocito, D., 2014. Energy measurement and fragment identification using digital signals from partially depleted Si detectors. Eur. Phys. J. A 50. https://doi.org/10.1140/epja/i2014-14086-9.

Pomorski, M., Berdermann, E., de Boer, W., Furgeri, A., Sander, C., Morse, J., 2007. Charge transport properties of single crystal CVD-diamond particle detectors. Diam. Relat. Mater. 16, 1066–1069. https://doi.org/10.1016/j.diamond.2006.11.016.

Topkar, A., Singh, A., Santra, S., Mukhopadhyay, P.K., Chatterjee, A., Choudhury, R.K., Pithawa, C.K., 2011. Development of integrated ΔE–E silicon detector telescope using silicon planar technology. Nucl. Instruments Methods Phys. Res. Sect. A Accel. Spectrometers, Detect. Assoc. Equip. 654, 330–335. https://doi.org/10.1016/j.nima.2011.07.001.

Tran, L.T., Bolst, D., Guatelli, S., Biasi, G., Fazzi, A., Sagia, E., Prokopovich, D.A., Reinhard, M.I., Keat, Y.C., Petasecca, M., Lerch, M.L.F., Pola, A., Agosteo, S., Matsufuji, N., Jackson, M., Rosenfeld, A.B., 2018. High spatial resolution microdosimetry with monolithic ΔE-E detector on 12C beam: Monte Carlo simulations and experiment. Nucl. Instruments Methods Phys. Res. Sect. A Accel. Spectrometers, Detect. Assoc. Equip. 887, 70–80. https://doi.org/10.1016/j.nima.2017.12.079.

Verona, C., Magrin, G., Solevi, P., Bandorf, M., Marinelli, M., Stock, M., Rinati, G.V., 2018. Toward the use of single crystal diamond based detector for ion-beam therapy microdosimetry. Radiat. Meas. 110, 25–31. https://doi.org/10.1016/j.radmeas.2018.02.001.

Wroe, A., Schulte, R., Fazzi, A., Pola, A., Agosteo, S., Rosenfeld, A., 2009. RBE estimation of proton radiation fields using a DeltaE-E telescope. Med. Phys. 36, 4486–4494. https://doi.org/10.1118/1.3215927.

Zahradnik, I.A., Pomorski, M.T., De Marzi, L., Tromson, D., Barberet, P., Skukan, N., Bergonzo, P., Devès, G., Herault, J., Kada, W., Pourcher, T., Saada, S., 2018. scCVD

diamond membrane based microdosimeter for hadron therapy. Phys. Status Solidi 215. https://doi.org/10.1002/pssa.201800383.

Zhu, Z., Yu, M., Jin, Y., 2021. Fabrication of integrated silicon PIN detector based on Al-Sn-Al bonding for ΔE-E telescope application. Microelectron. Eng. 247 https://doi.org/10.1016/j.mee.2021.111599.

Ziegler, J.F., Ziegler, M.D., Biersack, J.P., 2010. SRIM – the stopping and range of ions in matter (2010). Nucl. Instrum. Methods Phys. Res. Sect. B Beam Interact. Mater. Atoms 268, 1818–1823. https://doi.org/10.1016/j.nimb.2010.02.091.